Wear 524-525 (2023) 204896

Contents lists available at ScienceDirect

Wear

journal homepage: www.elsevier.com/locate/wear

Predicting rail corrugation in a real line by means of a fast non-linear vertical and lateral model

Rakel Robles, Nekane Correa *, Ernesto G. Vadillo, Julio Blanco-Lorenzo

Department of Mechanical Engineering, University of the Basque Country UPV/EHU, Escuela de Ingeniería de Bilbao, Plaza Torres Quevedo 1, 48013, Bilbao, Spain

ARTICLE INFO

Keywords:
Rail corrugation
Experimental measurements
Track receptances
Rail dynamics
Wheel-rail contact
Wear

ABSTRACT

This work is the result of a problem of premature development of rail corrugation found on a new metro line. As urgent solutions, a rail grinding was carried out and friction modifier started to be applied. Experimental corrugation measurements have been taken periodically in this line at 60 control points since 2018, and an extensive database has been collected since then. As a second stage, a computationally efficient new model has been developed to predict corrugation growth under different running conditions. The aim of this work has been to obtain feasible solutions to delay corrugation growth in metro type lines.

1. Introduction

When vehicles pass over the track, fluctuating contact forces are generated. These forces induce wear, thus producing irregularities on the rail surface, such as corrugation. It is known that rail irregularities such as welds [1,2] can act as a trigger for corrugation development, which can lead to the development of other type of irregularities including rolling contact fatigue (RCF) [3–5]. Corrugation causes significant noise and vibration problems [6,7] and reduces the service life of both the track and the vehicle, so it is a subject on which a large number of studies have been carried out over time.

Different types of corrugation are distinguished by their wavelength fixing mechanism and damage fixing mechanism, as described by Grassie in Ref. [8]. In this work, experimental measurements of rail corrugation have been carried out in a metro type line. This corrugation was mainly found on the inner rail of the curves with a wavelength of about 5 cm.

The only solution to eliminate the corrugation of the rail surface is to carry out a grinding process [9]. As this procedure entails high costs, different alternative methods have been studied to eliminate or at least reduce the rate of corrugation growth. The measures against corrugation can be divided into preventive and corrective measures, depending on when the selected measure is adopted. Therefore, preventive measures, which include preventive grinding and dynamic optimization of the track components [10], are implemented before the opening of the line; and corrective measures are adopted when the line is operational. These corrective measures comprise modification of sleepers spacing [11], modification of pad stiffness [12,13], use of friction modifiers [14–17], or variability of the vehicle's speed [18,19].

In this article, a complete study of corrugation is carried out in a new metro line located in the surroundings of Bilbao. This study was initiated due to the rapid development of corrugation within the first three months after the line's inauguration. Due to this early corrugation growth, two urgent measures were taken: rail grinding and high positive friction (HPF) modifier implementation. Rail geometry and corrugation measurements have been carried out periodically on this line since 2018 so that an extensive database of 60 control points is now available. In parallel, a more intensive study has been developed to obtain possible solutions to the early growth of corrugation. For this purpose, a new model has been developed by the authors to predict track wear after a specific number of wheelsets passes.

Different models have been developed in the past to study corrugation, classified as models in the frequency domain and in the time-domain. Frequency domain models [20–24] are linear models that can achieve very accurate results in a reduced time. On the other hand, the time-domain models [25–30] require longer computational time since, for each of the wheelset passes, the system of equations defining the problem has to be solved.

The model described in this article is a model in the time/space domain, since a non-linear contact between wheel and rail is considered. This new model uses a methodology similar to that described by Wu in Refs. [31–33] and Correa in Refs. [34,35], in which the rational fraction

* Corresponding author.
E-mail address: nekane.correa@ehu.es (N. Correa).

https://doi.org/10.1016/j.wear.2023.204896
Received 12 January 2023; Received in revised form 14 March 2023; Accepted 31 March 2023
Available online 1 April 2023

polynomials (RFP) method is used to fit track dynamics. In the mentioned models, the receptances of the track are different at each of the positions along the span. These differences are due to the discrete support of the sleepers. Thus, the dynamic characteristics of the track are taken into account accurately. These include the influence of the railpad, sleepers, boots and ballast, including their mass, stiffness and damping.

The new model's advantage, but also the main challenge, lies in incorporating the lateral dynamics into the system of equations since it has been demonstrated to be crucial, especially in sharp curves [36]. All this without compromising the low computation time. This new model is developed and validated in Ref. [37] with corrugation data measured experimentally from the line, and, as already mentioned, it is used to predict corrugation growth under different running conditions.

The article is divided into seven sections. This first section describes the problem, and briefly presents the line in which the study is carried out and the model developed to predict its evolution. In the following sections, the problem is identified (section 2) and the line is described (section 3). Then, experimental measurements and possible solutions are presented (section 4). Next, wear growth on the line is predicted by modelling, adapting a new model developed in the time/space domain to the line under study (section 5). Finally, wear results are presented under different running conditions (section 6), and the conclusions of the present work are discussed (section 7).

2. Problem identification

In mid-2017, a new metro line was inaugurated in the vicinity of Bilbao. After barely three months of vehicles circulation, corrugation had already developed along the line, increasing noise levels and vibrations. The corrugation formation also caused problems in passenger comfort and led to complaints from nearby residents.

Due to this problem, the authors started a corrugation study in this line. The main objective of this study was to obtain viable solutions to reduce the corrugation growth rate and to identify the core reasons for premature corrugation development.

This corrugation study initiated at the end of 2017, and is still ongoing at present to assess the effectivity of the implemented measures.

3. Line description

As already mentioned, the metro line on which the corrugation study was carried out is located in the outskirts of Bilbao and consists of 8.5 km of double track including seven stations. It is a slab track with discrete support, in which the distances between sleepers are among 0.6 and 1 m, depending on the circular curve's radius. The minimum radius in this line is 150 m, and the rails are 54E1 with SKL-1 fastenings. Vehicles running on the line consist of 3 or 4 cars and run every 7.5 min.

The rail hardness varies in the line taking two different values since part of an old-line running in the same area was reused. Thus, in the reused track area, the rail hardness grade is R260, and in the new area, a hardened rail with a hardness grade of R350HT is used.

The maximum noise level endured by passengers waiting on the platform at one of the stations was 99.9 dB (A). This noise level was measured experimentally with a precision sound level meter (Brüel & Kjaer 2250), as shown in Fig. 1.

4. Solutions

The solutions presented in this work are classified into two groups. On the one hand, urgent measures were taken to eliminate the existing corrugation in the line. On the other hand, a long-term study has been carried out to obtain possible alternatives to delay or eliminate the corrugation growth.

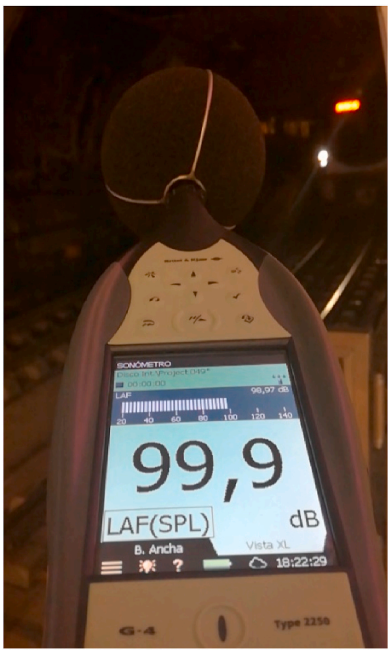

Fig. 1. Measured noise level in a station.

4.1. Urgent measures

Due to the early corrugation development after only 175,000 wheelset passes since the line's opening, two measures were taken as a matter of urgency. The first measure consisted in grinding the track, and the second was the implementation of HPF. Both measures were taken prior to the experimental measurements and proved essential in reducing the corrugation growth rate.

The grinding process was carried out a few months after the commissioning of the line. In that short period, corrugation had already developed (Fig. 2). All rail grindings have kept the rail profile

Fig. 2. Corrugation found in the line under study.

unchanged. The first corrective grinding proved to be essential, since not only eliminated the existing corrugation, but also delayed the subsequent development of corrugation in the line, allowing to extend the period of time until the next grinding. Thus, the subsequent grinding was done approximately 2 million wheelset passes after, allowing us to study the evolution of the corrugation throughout this period.

Friction modifier was not initially applied in this line. Its implementation proved to be of great relevance since the corrugation growth rate decreased significantly since then.

4.2. Long-term solutions

After the necessary urgent measures, experimental measurements were taken from the track to study viable and easily applicable solutions to eliminate or at least reduce the corrugation growth.

4.2.1. Corrugation experimental study

The study of corrugation on the new metro line started at the end of 2017. Firstly, the methodology for corrugation monitoring was proposed. After analyzing the track characteristics, 60 control points located on circular curves were selected. Thus, the experimental measurements of rail geometry and corrugation in these control points started in early 2018. Fig. 3 shows the complete line with the selected kilometer points marked with a red dot. In this kilometer points measurements were taken in both tracks. Some of the most representative control points are identified in the figure with the letters A, B, C and D. These points are described further on.

The experimental measurements were carried out using an R2S rail surface scanner from Metalelektro, which is shown in Fig. 4.

The mentioned 60 control points can be classified into two different

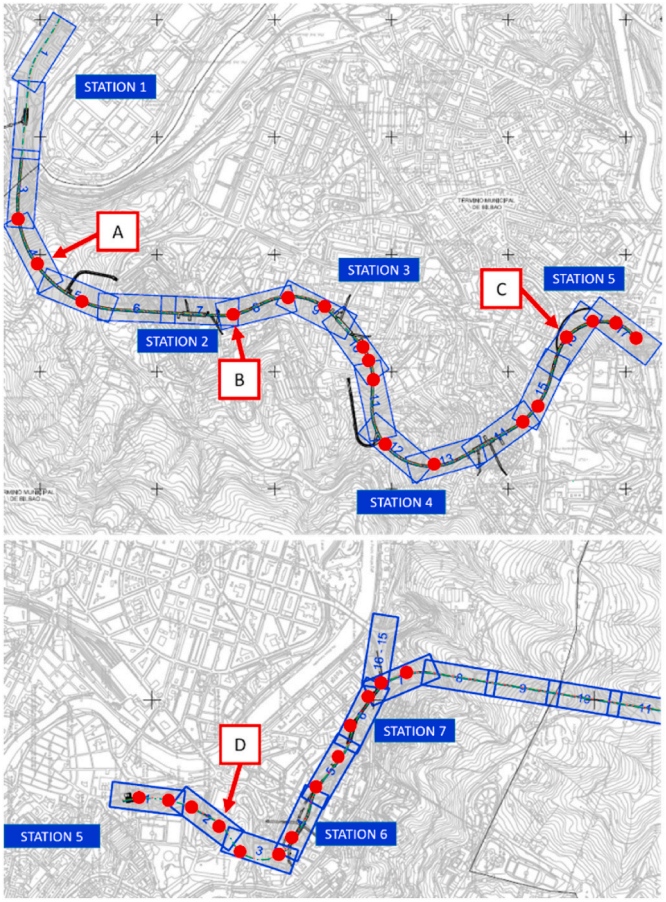

Fig. 3. Line under study.

Fig. 4. Corrugation measurement device (R2S).

groups depending on their corrugation evolution. The first group points (Group 1) are those where rail corrugation has not developed and constitutes approximately 40% of the control points studied. The second group points (Group 2), the remaining 60%, show a development of corrugation with the increasing number of wheelset passes.

The most representative control points of both groups have been selected (A, B and C). The corrugation evolution of these points is shown in Figs. 5–7. The number of wheelset passes displayed in the legends of the following figures is measured after the first grinding.

The first point (point A) is representative of those control points where corrugation has not developed (Group 1). Most of these points have radii of curvature above 300 m, in this particular case being 450 m. Fig. 5 shows the absence of corrugation at this particular point.

Group 2 is represented by point B, which shows moderate corrugation growth (Fig. 6). At this point, the radius of curvature is 250 m and has a corrugation wavelength of 0.053 m after 1,775,000 wheelset passes. The majority of the points measured along the line, where corrugation has developed, have similar characteristics: radii of curvature below 200 m and wavelengths between 0.04 and 0.06 m. There are few exceptions where slightly shorter (0.036 m) and longer (0.067 cm) wavelengths were found.

Finally, Fig. 7 shows the corrugation measured at point C. The characteristics of this control point are as follows: radius of curvature of 198 m and wavelength of 0.053 m. Due to its characteristics, this control point belongs to Group 2, although it stands out for its greater corrugation growth. Hence, point C is representative of those points that experienced the most significant growth. At this control point, the maximum peak-to-peak value has increased by about 64 μm since the beginning of the measurements. This figure (Fig. 7) shows the positive effect of the urgent measures adopted since after almost 2 million passes, corrugation does not reach very high levels.

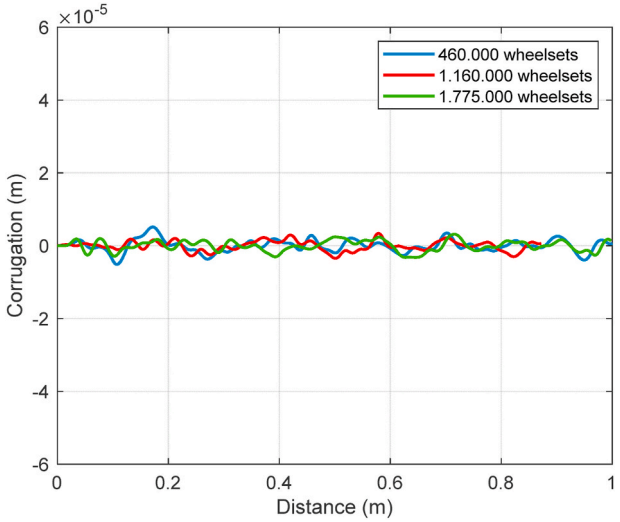

Fig. 5. Rail surface geometry in control point A.

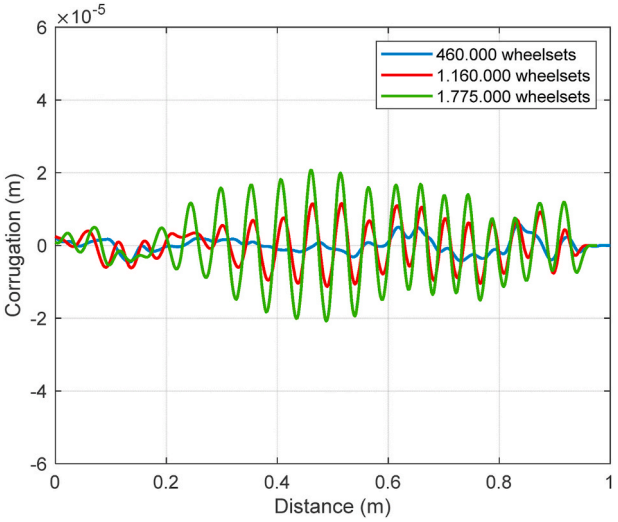

Fig. 6. Rail corrugation in control point B.

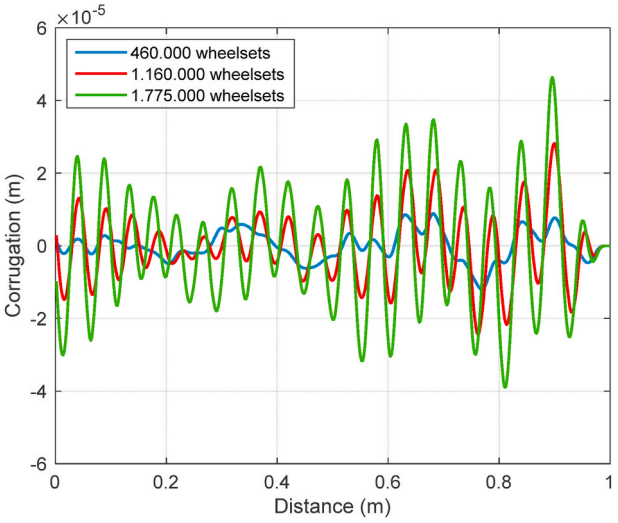

Fig. 7. Rail corrugation in control point C.

In summary, most of the control points showing corrugation are located on curves with radii less than 200 m and have wavelengths of around 0.05 m.

4.2.2. Diagnosis of the track parameters causing corrugation

As for longer-term solutions to corrugation, the modification of track parameters is studied. However, as this is a STEDEF track, neither the parameters of the boots nor the distance between sleepers can be modified easily. A possible modification for this type of track could be changing the railpads. In order to study the dynamic characteristics of the actual railpads, first, a sufficiently representative point of the corrugation evolution has been selected (point D).

In the selected point, the distance between sleepers is 0.64 m, and the curvature radius is 150 m. Fig. 8 shows the experimentally measured corrugation at this point for different number of wheelset passes. The wavelength found at this control point is around 5 cm.

To analyze the dynamic characteristics of the track, vertical and lateral track receptances are measured experimentally at point D. Since the track support is discrete, receptances are measured every 8 cm from the sleeper to the midspan. These receptances are measured by experimental impact testing using the following tools: instrumented hammer (PCB 086D05), accelerometers (PCB 352C33 ICP), analyzer (LMS Scadas

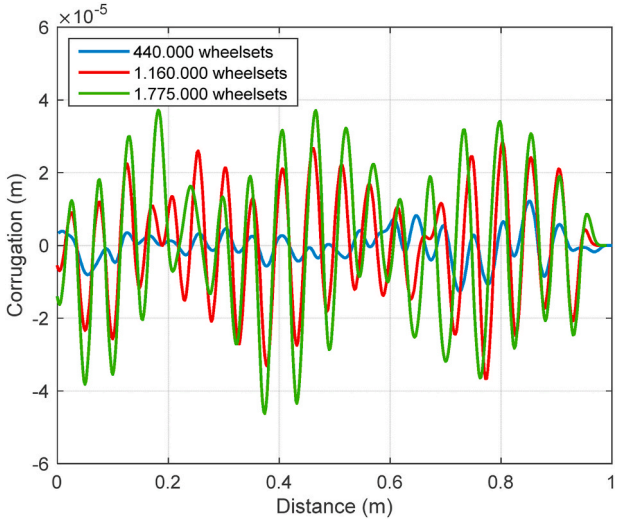

Fig. 8. Corrugation growth in control point D.

Mobile SCM05) and impact testing software (TestLab 17.1).

Figs. 9 and 10 show the vertical and lateral receptances for the positions: over sleeper (0 cm), quarter-span (16 cm) and midspan (32 cm). As can be seen in Figs. 9 and 3 peaks can be distinguished, which are associated with the boot mode (120 Hz), the pad mode (740 Hz), and the pinned-pinned mode (920 Hz).

The receptances displayed in Fig. 9 show a high stiffness of the railpad. This is confirmed by the dynamic stiffness measurements made by the manufacturer (1000 MN/m) and by the static stiffness measurements made in the workshop of the Department of Mechanical Engineering of the University of the Basque Country (800 MN/m). This stiffness value allows classifying these railpads as extremely stiff [38]. Different authors have studied this characteristic, so it is known that with lower pad stiffness, the corrugation develops more slowly [12,13]. Additionally, the wavelength found at this control point is related to the first antirresonance in the vertical direction. Thus, this is the wavelength fixing mechanism in this metro line. This antirresonance is fundamentally related to the railpads stiffness and the mass of the sleepers. A reduction of the railpad stiffness would produce a displacement of this peak in frequency. Thus, this change is expected to reduce the corrugation growth rate. For this reason, a change of railpads to ones with lower stiffness is currently being prepared in the line under study.

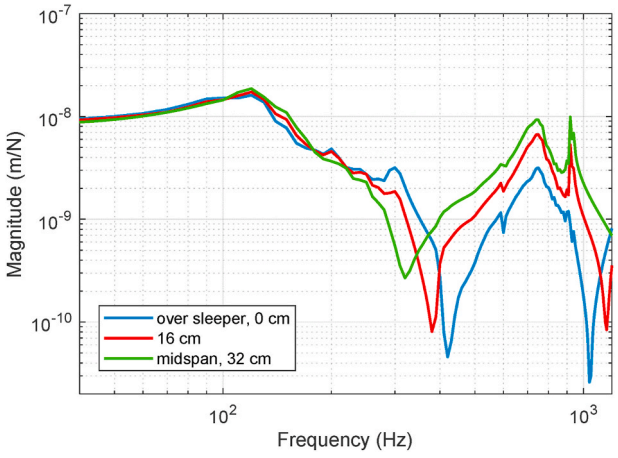

Fig. 9. Experimental vertical receptances of the track in different positions along the span.

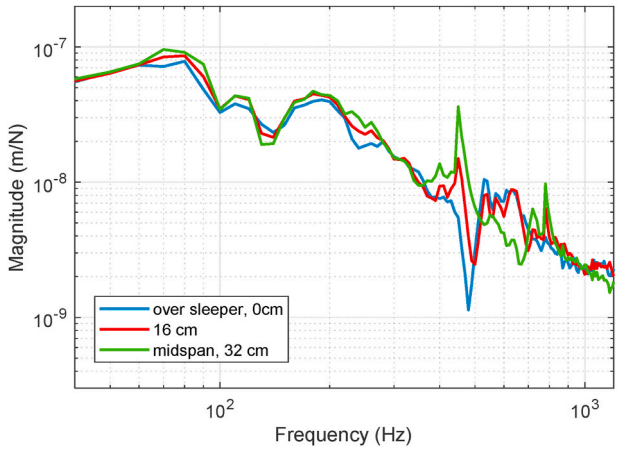

Fig. 10. Experimental lateral receptances of the track in different positions along the span.

5. Development of a new model for the prediction of rail corrugation

Up to this section, possible alternatives for reducing corrugation growth in a specific metro-type line have been studied. In parallel, a new model developed by the authors has been used to predict wear growth [37]. This model is already validated with the experimental corrugation measurements taken from the track at point D, and it is used to study wear evolution after a specific number of wheelset passes.

5.1. Model description

This section describes the model developed by the authors in Ref. [37], which is an efficient tool to predict wear growth in a specific line, under defined running conditions.

The receptances required as input to this model can be obtained in different ways: FEM, experimental measurements, or other mathematical tools. In this case, as already mentioned, the rail receptances have been measured experimentally at point D. The RFP method is used to obtain the coefficients (a and b) of the transfer function (Equation (1)) that fits each of the measured or calculated receptances.

An optimization is performed through multiobjective genetic algorithms to ensure the minimum error in the fitting and stability over time. Due to the variation of the receptances along the span, a linear variation of the transfer function coefficients is considered for the positions in between the fitted sections (in this particular case, the fitted sections are every 8 cm). Moreover, the track is considered as periodic in this model; therefore, the coefficients of the transfer function also vary periodically from one span to another.

$$R(s)=\frac{B(s)}{A(s)}=\frac{b_1 s^n+b_2 s^{n-1}+\cdots+b_{n-1}s+b_n}{s^m+a_1 s^{m-1}+a_2 s^{m-2}+\cdots+a_{m-1}s+a_m} \tag{1}$$

The orders of the polynomials of the transfer functions (n and m) are different for vertical and lateral dynamics. In general, the orders of the polynomials in lateral dynamics are higher than in vertical dynamics due to greater flexibility in this direction.

The equations to be solved include rail dynamics, wheel dynamics, and the interaction between the wheel and the rail. These equations are described in the following sections.

5.1.1. Track dynamics

Once the vertical and lateral fits of the rail are obtained, the Laplace transform is used to obtain an equation of order m, which is transformed into m equations of order 1 (Equation 2). Equation 2 has been generalized for any of the axes, where f(t) represents the wheel-rail contact force, and x1(t) is the rail displacement.

The following values are different for the vertical and lateral dynamics: contact force (f(t)), matrices **M** and ***c*** (Equations (3) and (4)), orders of the polynomials (n and m) and coefficients of the polynomials (a and b). With this in mind, both equations of the rail are obtained from the fitting of each of the receptances.

$$\dot{\mathbf{x}}(\mathbf{t})=\mathbf{M}*\mathbf{x}(\mathbf{t})+\mathbf{c}*f(t) \tag{2.1}$$

$$\mathbf{x}(\mathbf{t})=\begin{Bmatrix} x_1(t)\\ x_2(t)\\ \cdots\\ x_m(t)\end{Bmatrix} \tag{2.2}$$

$$\mathbf{M}=\begin{bmatrix} 0 & 1 & 0 & \cdots & 0\\ 0 & 0 & 1 & \cdots & 0\\ 0 & 0 & 0 & \cdots & 0\\ \cdots & \cdots & \cdots & \cdots & \cdots\\ -a_m & -a_{(m-1)} & -a_{(m-2)} & \cdots & -a_1\end{bmatrix} \tag{3}$$

$$\mathbf{c}=\begin{Bmatrix} b_1\\ b_2-a_1*b_1\\ \cdots\\ b_m-\sum_{k=1}^{m-1}a_{(m-k)}*c_k\end{Bmatrix} \tag{4}$$

5.1.2. Wheel dynamics and wheel-rail interaction

In previous works, the vertical (z-axis) model of the wheel was based on a concentrated mass to which the part of the vehicle weight supported by the wheel is applied. In this case, since experimental measurements of the wheel vertical receptance have been obtained, the vertical model of the wheel is achieved by fitting this wheel vertical receptance, using Equations (1)–(4).

The vertical force of the wheel-rail contact is calculated as shown in Equation (5). In this equation, C_H is the Hertz coefficient, z_w the vertical displacement of the wheel, z_r the vertical displacement of the rail and r the irregularity of the rail profile. The vertical axis (z-axis) is considered positive in case of a dip and negative in case of a protrusion.

$$f_c(t)=\begin{cases} C_H*(z_w(t)-z_r(t)-r(t))^{\frac{3}{2}}, \text{when } (z_w(t)-z_r(t)-r(t))>0\\ 0, \text{when } (z_w(t)-z_r(t)-r(t))\le 0\end{cases} \tag{5}$$

In the lateral direction (y-axis), wheel dynamics has been added to the system of equations by fitting the experimentally measured wheel lateral receptance, using Equations (1)–(4). Lateral dynamics equations have been completed with Equation (6), in which the variability of the lateral creepage (γ_y) is considered from its nominal value (γ_{y0}). In this equation, $\dot{y}_w$ represents the lateral displacement velocity of the wheel, $\dot{y}_r$ the lateral displacement velocity of the rail and V is the vehicle running speed.

$$\gamma_y=\gamma_{y0}+\frac{\dot{y}_w(t)-\dot{y}_r(t)}{V} \tag{6}$$

5.1.3. Wear calculation

Wear is considered to be proportional to the friction power, and is calculated by Equation (7). In this equation, z is the function representing the longitudinal profile of the track, k_0 is the wear constant, q is the tangential stress at each point of the contact patch, s is the sliding module, ρ is the steel density, and V is the vehicle driving speed. Δx represents the magnitude of the discretization of the contact patch in the longitudinal direction, which is used to calculate the tangential stresses.

$$\Delta z=\frac{k_0 q s \Delta x}{\rho V} \tag{7}$$

There are different methods to calculate the tangential stresses in the wheel-rail contact [39,40]. In this article, the FASTSIM algorithm is used, since it has been proved to be accurate enough.

5.2. Model implementation

The new model has been adapted for the described line. Experimentally measured receptances have been fitted at the selected point as described in the previous section. The orders of the polynomials of the vertical and lateral receptances of the track are 9 and 10, and 11 and 12, respectively.

Vertical and lateral track receptances fittings are shown in Figs. 11 and 12. The fitting has been made for the five positions within the span, although only the fitting over the sleeper and at midspan have been included for space reasons.

The experimentally measured wheel receptances have been fitted likewise to the track receptances, the value of m being equal to 10 vertically and 12 laterally. Figs. 13 and 14 show the wheel receptances and its fittings.

To compare the corrugation growth obtained from the experimental measurements with model results, wear has been calculated from the initial irregularity shown in Fig. 15, related to the rail surface irregularity measured experimentally after a rail grinding. In addition, as the driving speed is variable following a normal distribution with a mean value of 53.6 km/h and a standard deviation of 2.8 km/h, random speeds following this distribution have been considered.

The wear coefficient has been obtained from literature data [42], where different wear coefficients are calculated for different values of longitudinal creepage. Thus, for the studied curve, the value of k_0 is around 5e-10 kg/Nm for a track of grade R260, without lubrication and whose friction coefficient is 0.45. In Ref. [43], it is observed that the wear coefficient for R260 grade rails is about 4 times higher than for the case of R350HT grade rails. On the other hand, in Ref. [41], Vuong et al. concluded that the wear coefficient is almost 5 times higher when no friction modifier is used than when HPF is used. Therefore, the wear coefficient value used for the following simulations is 3e-11 kg/Nm, as it is a track with hardness grade R350HT where HPF is applied. In this work, the value of C_H is 93.03 GN m$^{-3/2}$.

Fig. 16 compares the calculated corrugation with that obtained from

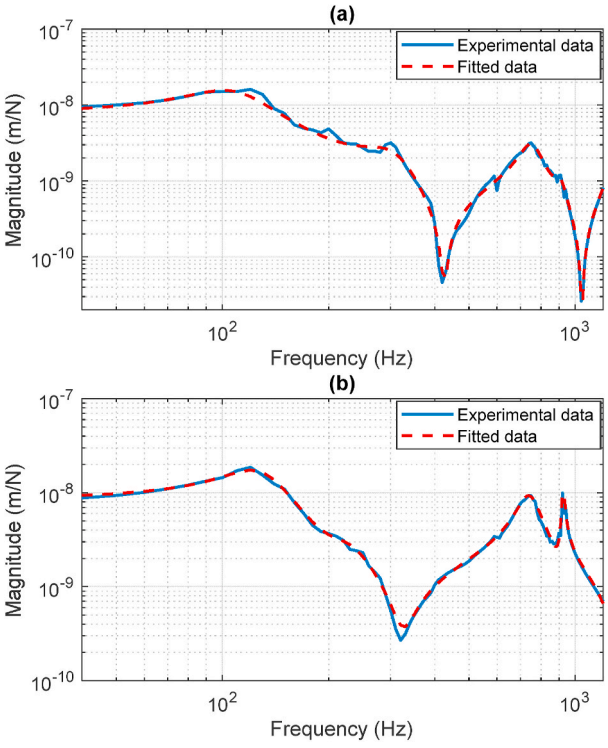

Fig. 11. Experimental and fitted vertical receptances of the track: (a) over the sleeper, (b) at midspan.

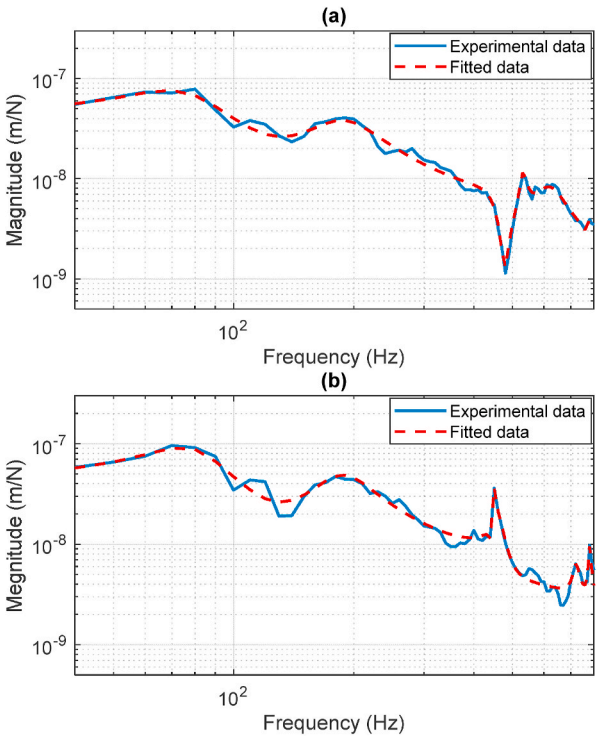

Fig. 12. Experimental and fitted lateral receptances of the track: (a) over the sleeper, (b) at midspan.

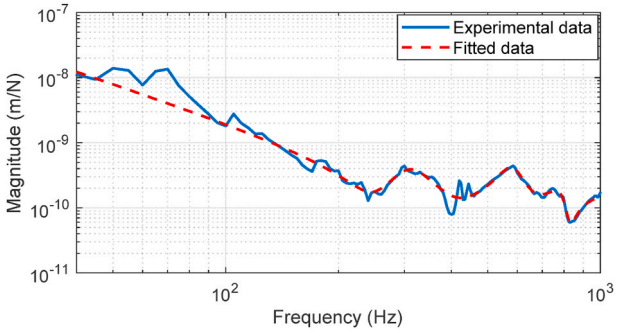

Fig. 13. Experimental and fitted vertical receptance of the wheelset.

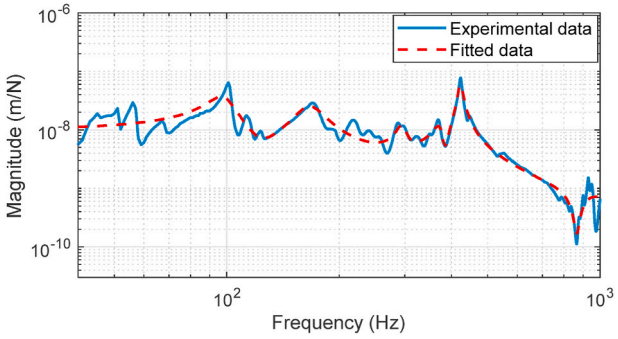

Fig. 14. Experimental and fitted lateral receptance of the wheelset.

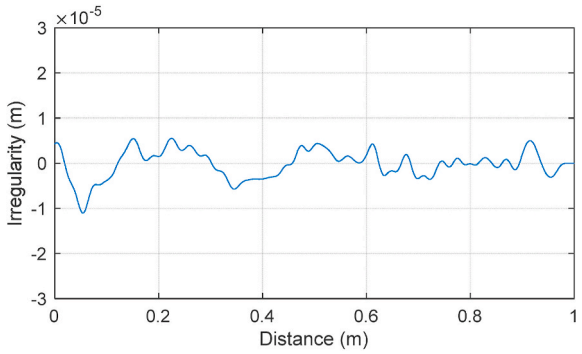

Fig. 15. Initial irregularity.

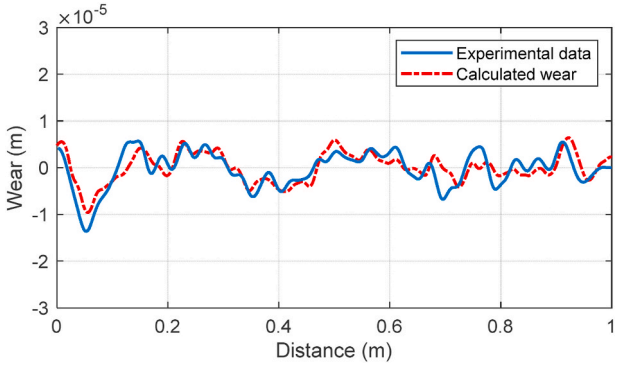

Fig. 16. Comparison between experimental measurement and calculated wear.

experimental measurements 183,000 wheelset passes after the grinding. Significant similarity is observed in both amplitudes and wavelengths.

6. Prediction of wear evolution under different running conditions

The model described in this article is used to predict the corrugation growth on a given line with defined circulation conditions, after a specific number of wheelset passes.

To reduce or eliminate the corrugation growth in the line under study, different running conditions are analyzed. For this purpose, the speed distribution and the friction coefficient in the wheel-rail contact have been modified. The following sections show the wear evolution obtained with the model for the different running conditions mentioned above.

6.1. Speed distribution variation

In studies by Bellette and Meehan in Refs. [18,19], it is proved that the greater the variation in vehicle speed, the lower the corrugation growth rate. As the vehicles running on this metro-type line do not operate with ATO, it is possible for the drivers to vary the speed so that the same rail frequencies are not continuously excited, thus slowing down the development or growth of corrugation.

As already mentioned, the average speed at which vehicles run through point D is 53.6 km/h. To study the effect of speed variability on wear, three different scenarios have been assumed. First, a constant speed equal to 53.6 km/h is considered to compare the corrugation evolution in case the ATO system was in operation. The second scenario represents the speed at which vehicles currently travel on the line. This distribution is described in the previous section. A larger deviation has been considered for the third speed distribution, thus moving further away from the mean value. In this last speed distribution, the average value is 53.6 km/h and the standard deviation is 5 km/h.

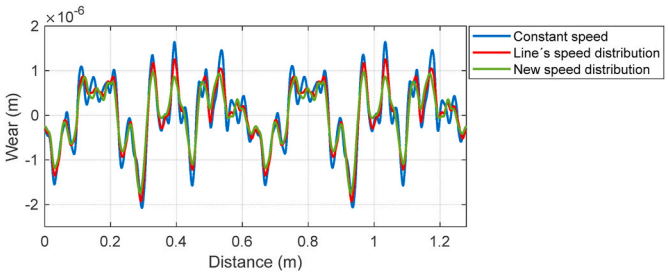

Fig. 17. Wear growth after 100,000 passovers with different speed distributions.

In Fig. 17 the calculated wear after 100,000 wheelset passages is presented for the 3 different speed distributions. As expected, the corrugation wavy shape develops more rapidly when the vehicle speed is constant (blue line). It is also observed that increasing the deviation in the velocity distribution (green line) delays the wear development. Moreover, in the cases in which speed variability is considered the predominant wavelengths are of 5.2 and 7 cm, whereas with constant speed a smaller wavelength emerges (3.5 cm), in addition to the above two.

This result is of great interest since increasing slightly the deviation of the speed distribution through the different curves would reduce corrugation growth without a significant service change.

6.2. Friction coefficient variation

The friction coefficient between the wheel and the rail depends on the materials in contact and other aspects, such as friction modifiers or lubricants. For this reason, the effect of different friction coefficient values on wear evolution have been studied: 0.3, 0.4, and 0.5. The aforementioned range is the usual range of friction coefficient values in the wheel-rail contact.

In the figure below, wear has been calculated with the current speed distribution over 100,000 wheelset passes, for the different friction coefficients. Fig. 18 shows that the higher the friction coefficient, the higher the corrugation growth. Therefore, it is essential to maintain the friction coefficient at levels close to 0.3 since this significantly reduces the amplitude of wear and lowers the rate of corrugation growth. The predominant wavelengths in Fig. 18 are of 5.2 and 7 cm, as in the previous cases, although with greater amplitude.

7. Conclusions

This article contains the results of a 5-year experimental corrugation study on a metro line in the Bilbao area. In this line, corrugation appeared prematurely after its inauguration. Experimental measurements of the rail surface corrugation started after taking two urgent measures: rail grinding and HPF implementation. The aforementioned control measures appeared to be indispensable for reducing corrugation

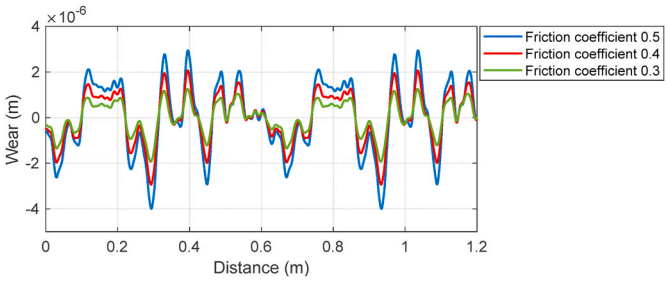

Fig. 18. Wear growth after 100,000 passovers with different friction coefficients.

growth rate along the entire line.

This work shows the corrugation growth at different control points, which are representative of the growth that has been found along the line, taking into account the wavelengths and radii of curvature. The control point D, which has been considered sufficiently representative, has been selected to carry out a more in-depth study of the development of corrugation. At this point, experimental measurements of both vertical and lateral track receptances have been carried out to study possible modifications of track parameters to reduce the corrugation growth rate. In the measured receptances a high railpad stiffness has been observed. It is known from the literature that lower pad stiffness reduces the corrugation growth rate and decreases rolling noise. For this reason, a change of railpads is currently being arranged.

A new time/space domain model has been developed by the authors to predict the development of corrugation. This new model fits the vertical and lateral receptances of the track and the wheel through transfer functions. The remarkable implication of lateral dynamics in wear is demonstrated, mainly in sharp curves. Transfer functions are transformed into systems of equations describing the track and wheel dynamics, which are completed with the equations defining the contact between the two bodies. Wear is calculated by considering it proportional to the friction power.

This model is adapted to the line under study, more specifically to point D. Wear is calculated under different running conditions, considering different vehicle speed distributions and coefficients of friction between the bodies. The different speed distributions show that the greater the deviation, the smaller the extent of wear and the less corrugation is developed. This measurement can be easily applied on the line since, not running with ATO, the driver selects the speed at which the vehicle runs through each of the curves. Regarding the different friction coefficients studied, it has been observed that the best result is obtained with a value of 0.3, showing less wear amplitude.

Credit author statement

Rakel Robles: Methodology, Experimental measurements, Model development & validation, Analysis, Writing – original draft, Writing – review & editing. **Nekane Correa:** Methodology, Supervision, Experimental measurements, Writing – review & editing. **Ernesto G. Vadillo:** Methodology, Supervision, Experimental measurements, Writing – review & editing. **Julio Blanco-Lorenzo:** Analysis, Validation.

Declaration of competing interest

The authors declare that they have no known competing financial interests or personal relationships that could have appeared to influence the work reported in this paper.

Data availability

Data will be made available on request.

Acknowledgments

The authors gratefully acknowledge financial support from the European Horizon 2020 Joint Technology Initiative Shift2Rail (IN2TRACK3) [101012456], from the Spanish Research Ministry MICINN/Economy and Competitiveness Ministry MINECO and MCI/AEI [PID2019-109483RB-I00], including funding by the FEDER-ERDF European Regional Development Fund, and from the Basque Government [IT1764-22, PRE_2021_2_0047, KK-2023/00029].

References

[1] M.J.M.M. Steenbergen, Quantification of dynamic wheel–rail contact forces at short rail irregularities and application to measured rail welds, J. Sound Vib. 312 (2008) 606–629, https://doi.org/10.1016/j.jsv.2007.11.004.
[2] Z. Wen, G. Xiao, X. Xiao, X. Jin, M. Zhu, Dynamic vehicle–track interaction and plastic deformation of rail at rail welds, Eng. Fail. Anal. 16 (2009) 1221–1237, https://doi.org/10.1016/j.engfailanal.2008.08.001.
[3] A. Ekberg, E. Kabo, J.C.O. Nielsen, R. Lundén, Subsurface initiated rolling contact fatigue of railway wheels as generated by rail corrugation, Int. J. Solid Struct. 44 (2007) 7975–7987, https://doi.org/10.1016/j.ijsolstr.2007.05.022.
[4] Z. Li, X. Zhao, C. Esveld, R. Dollevoet, M. Molodova, An investigation into the causes of squats—correlation analysis and numerical modeling, Wear 265 (2008) 1349–1355, https://doi.org/10.1016/j.wear.2008.02.037.
[5] V.V. Krishna, S. Hossein-Nia, C. Casanueva, S. Stichel, G. Trummer, K. Six, Rail RCF damage quantification and comparison for different damage models, Railw. Eng. Sci. (2022) 23–40, https://doi.org/10.1007/s40534-021-00253-y.
[6] J. Han, X. Xiao, Y. Wu, Z. Wen, G. Zhao, Effect of rail corrugation on metro interior noise and its control, Appl. Acoust. 130 (2018) 63–70, https://doi.org/10.1016/j.apacoust.2017.09.007.
[7] T. Xin, S. Wang, L. Gao, H. Huo, Y. Ding, P. Wang, P. Chen, P. Liu, Field measurement of rail corrugation influence on environmental noise and vibration: a case study in China, Meas.: J. Int. Meas. Confed. 164 (2020), 108084, https://doi.org/10.1016/j.measurement.2020.108084.
[8] S.L. Grassie, Rail corrugation: characteristics, causes and treatments, J. Rail and Rapid Transit 223 (2009) 581–596, https://doi.org/10.1243/09544097JRRT264.
[9] J. Kalousek, P. Sroba, C. Hegelund, Analysis of Rail Grinding Tests and Implications for Corrective and Preventative Grinding, 4th Heavy Haul Railway Conference 1989, Railways in Action, 1989, pp. 193–204.
[10] O. Oyarzabal, J. Gómez, J. Santamaría, E.G. Vadillo, Dynamic optimization of track components to minimize rail corrugation, J. Sound Vib. 319 (2009) 904–917, https://doi.org/10.1016/j.jsv.2008.06.020.
[11] E.G. Vadillo, J.A. Tárrago, G. Garate, C.A. Duque, Effect of sleeper distance on rail corrugation, Wear 217 (1998) 140–146, https://doi.org/10.1016/S0043-1648(97)00239-1.
[12] H. Ilias, The influence of railpad stiffness on wheel/track interaction and corrugation growth, J. Sound Vib. 227 (1999) 935–948, https://doi.org/10.1006/jsvi.1999.2059.
[13] J.I. Egana, J. Vinolas, M. Seco, Investigation of the influence of rail pad stiffness on rail corrugation on a transit system, Wear 261 (2006) 216–224, https://doi.org/10.1016/j.wear.2005.10.004.
[14] D.T. Eadie, J. Kalousek, K.C. Chiddick, The role of high positive friction (HPF) modifier in the control of short pitch corrugations and related phenomena, Wear 253 (2002) 185–192, https://doi.org/10.1016/S0043-1648(02)00098-4.
[15] J.I. Egana, J. Vinolas, N. Gil-Negrete, Effect of liquid high positive friction (HPF) modifier on wheel-rail contact and rail corrugation, Tribol. Int. 38 (2005) 769–774, https://doi.org/10.1016/j.triboint.2004.11.006.
[16] W.J.T. Daniel, C.- Cheng, P.A. Meehan, Modelling the effects of friction modifiers on rail corrugation in cornering, Veh. Syst. Dyn. 46 (2008) 845–866, https://doi.org/10.1080/00423110701656767.
[17] R. Stock, L. Stanlake, C. Hardwick, M. Yu, D. Eadie, R. Lewis, Material concepts for top of rail friction management – classification, characterisation and application, Wear 366–367 (2016) 225–232, https://doi.org/10.1016/j.wear.2016.05.028.
[18] P.A. Bellette, P.A. Meehan, W.J.T. Daniel, Effects of variable pass speed on wear-type corrugation growth, J. Sound Vib. 314 (2008) 616–634, https://doi.org/10.1016/j.jsv.2007.12.038.
[19] P.A. Meehan, R.D. Batten, P.A. Bellette, The effect of non-uniform train speed distribution on rail corrugation growth in curves/corners, Wear 366–367 (2016) 27–37, https://doi.org/10.1016/j.wear.2016.05.009.
[20] K. Hempelmann, K. Knothe, An extended linear model for the prediction of short pitch corrugation, Wear 191 (1996) 161–169, https://doi.org/10.1016/0043-1648(95)06747-7.
[21] S. Mueller, A linear wheel–rail model to investigate stability and corrugation on straight track, Wear 243 (2000) 122–132, https://doi.org/10.1016/S0043-1648(00)00434-8.
[22] I. Gómez, E.G. Vadillo, A linear model to explain short pitch corrugation on rails, Wear 255 (2003) 1127–1142, https://doi.org/10.1016/s0043-1648(03)00282-5.
[23] J. Gómez, E.G. Vadillo, J. Santamaría, A comprehensive track model for the improvement of corrugation models, J. Sound Vib. 293 (2006) 522–534, https://doi.org/10.1016/j.jsv.2005.08.064.
[24] R.D. Batten, P.A. Bellette, P.A. Meehan, R.J. Horwood, W.J.T. Daniel, Field and theoretical investigation of the mechanism of corrugation wavelength fixation under speed variation, Wear 271 (2011) 278–286, https://doi.org/10.1016/j.wear.2010.10.027.
[25] L. Baeza, P. Vila, G. Xie, S.D. Iwnicki, Prediction of rail corrugation using a rotating flexible wheelset coupled with a flexible track model and a non-Hertzian/non-steady contact model, J. Sound Vib. 330 (2011) 4493–4507, https://doi.org/10.1016/j.jsv.2011.03.032.
[26] X. Sheng, X. Xiao, S. Zhang, The time domain moving Green function of a railway track and its application to wheel–rail interactions, J. Sound Vib. 377 (2016) 133–154, https://doi.org/10.1016/j.jsv.2016.05.011.
[27] T. Mazilu, Interaction between moving tandem wheels and an infinite rail with periodic supports – green's matrices of the track method in stationary reference frame, J. Sound Vib. 401 (2017) 233–254, https://doi.org/10.1016/j.jsv.2017.04.035.

[28] A. Carlberger, P.T. Torstensson, J.C. Nielsen, A. Frid, An iterative methodology for the prediction of dynamic vehicle–track interaction and long-term periodic rail wear, Proc. Inst. Mech. Eng. - Part F J. Rail Rapid Transit 232 (2018) 1718–1730, https://doi.org/10.1177/0954409717747127.
[29] S. Zhang, G. Cheng, X. Sheng, D.J. Thompson, Dynamic wheel-rail interaction at high speed based on time-domain moving Green's functions, J. Sound Vib. 488 (2020), 115632, https://doi.org/10.1016/j.jsv.2020.115632.
[30] M. Maglio, A. Pieringer, J.C.O. Nielsen, T. Vernersson, Wheel–rail impact loads and axle bending stress simulated for generic distributions and shapes of discrete wheel tread damage, J. Sound Vib. 502 (2021), 116085, https://doi.org/10.1016/j.jsv.2021.116085.
[31] T.X. Wu, D.J. Thompson, Theoretical investigation of wheel/rail non-linear interaction due to roughness excitation, Veh. Syst. Dyn. 34 (2000) 261–282, https://doi.org/10.1076/vesd.34.4.261.2060.
[32] T.X. Wu, D.J. Thompson, On the parametric excitation of the wheel/track system, J. Sound Vib. 278 (2004) 725–747, https://doi.org/10.1016/j.jsv.2003.10.047.
[33] T.X. Wu, Parametric excitation of wheel/track system and its effects on rail corrugation, Wear 265 (2008) 1176–1182, https://doi.org/10.1016/j.wear.2008.01.025.
[34] N. Correa, E.G. Vadillo, J. Santamaria, J. Gómez, A rational fraction polynomials model to study vertical dynamic wheel–rail interaction, J. Sound Vib. 331 (2012) 1844–1858, https://doi.org/10.1016/j.jsv.2011.12.012.
[35] N. Correa, E.G. Vadillo, J. Santamaria, J. Herreros, A versatile method in the space domain to study short-wave rail undulatory wear caused by rail surface defects, Wear 352–353 (2016) 196–208, https://doi.org/10.1016/j.wear.2016.02.012.
[36] M. Ishida, T. Moto, M. Takikawa, The effect of lateral creepage force on rail corrugation on low rail at sharp curves, Wear 253 (2002) 172–177, https://doi.org/10.1016/S0043-1648(02)00096-0.
[37] R. Robles, N. Correa, E.G. Vadillo, J. Blanco-Lorenzo, Comprehensive efficient vertical and lateral track dynamic model to study the evolution of rail corrugation in sharp curves, J. Sound Vib. 545 (2023), 117448, https://doi.org/10.1016/j.jsv.2022.117448.
[38] M. Oregui, A. de Man, M.F. Woldekidan, Z. Li, R. Dollevoet, Obtaining railpad properties via dynamic mechanical analysis, J. Sound Vib. 363 (2016) 460–472, https://doi.org/10.1016/j.jsv.2015.11.009.
[39] J.J. Kalker, A fast algorithm for the simplified theory of rolling contact, Veh. Syst. Dyn. 11 (1982) 1–13, https://doi.org/10.1080/00423118208968684.
[40] E.A.H. Vollebregt, P. Wilders, FASTSIM2: a second-order accurate frictional rolling contact algorithm, Comput. Mech. 47 (2010) 105–116, https://doi.org/10.1007/s00466-010-0536-7.
[41] T.T. Vuong, P.A. Meehan, D.T. Eadie, K. Oldknow, D. Elvidge, P.A. Bellette, W. J. Daniel, Investigation of a transitional wear model for wear and wear-type rail corrugation prediction, Wear 271 (2011) 287–298, https://doi.org/10.1016/j.wear.2010.10.008.
[42] B. Rodríguez, Nuevos desarrollos para la predicción de grietas en carriles ferroviarios por fatiga de contacto por rodadura, 2021.
[43] M. Mesaritis, J.F. Santa, L.F. Molina, M. Palacio, A. Toro, R. Lewis, Post-field grinding evaluation of different rail grades in full-scale wheel/rail laboratory tests, Tribol. Int. 177 (2023), 107980, https://doi.org/10.1016/j.triboint.2022.107980.